Computers & Geosciences 105 (2017) 51–64

Contents lists available at ScienceDirect

Computers & Geosciences

journal homepage: www.elsevier.com/locate/cageo

Research paper

Bayesian inference of spectral induced polarization parameters for laboratory complex resistivity measurements of rocks and soils

Charles L. Bérubé[a,*], Michel Chouteau[a], Pejman Shamsipour[a], Randolph J. Enkin[b], Gema R. Olivo[c]

[a] Polytechnique Montréal, Département des Génies Civil, Géologique et des Mines, Montréal, Québec, Canada
[b] Geological Survey of Canada – Pacific, Sidney, British Columbia, Canada
[c] Queen's University, Department of Geological Sciences and Geological Engineering, Kingston, Ontario, Canada

ARTICLE INFO

Keywords:
Spectral induced polarization
Petrophysics
Stochastic inversion
Markov chain Monte Carlo

ABSTRACT

Spectral induced polarization (SIP) measurements are now widely used to infer mineralogical or hydrogeological properties from the low-frequency electrical properties of the subsurface in both mineral exploration and environmental sciences. We present an open-source program that performs fast multi-model inversion of laboratory complex resistivity measurements using Markov-chain Monte Carlo simulation. Using this stochastic method, SIP parameters and their uncertainties may be obtained from the Cole-Cole and Dias models, or from the Debye and Warburg decomposition approaches. The program is tested on synthetic and laboratory data to show that the posterior distribution of a multiple Cole-Cole model is multimodal in particular cases. The Warburg and Debye decomposition approaches yield unique solutions in all cases. It is shown that an adaptive Metropolis algorithm performs faster and is less dependent on the initial parameter values than the Metropolis-Hastings step method when inverting SIP data through the decomposition schemes. There are no advantages in using an adaptive step method for well-defined Cole-Cole inversion. Finally, the influence of measurement noise on the recovered relaxation time distribution is explored. We provide the geophysics community with a open-source platform that can serve as a base for further developments in stochastic SIP data inversion and that may be used to perform parameter analysis with various SIP models.

1. Introduction

In recent years, there has been an increase in interest towards spectral induced polarization (SIP) to solve various problems in mineral exploration, hydrogeology, and environmental sciences. SIP data consists of complex resistivity measurements (phase shift and amplitude) in the frequency domain, typically between 1 mHz and 100 kHz. Mathematical models that describe SIP phenomena are often used to describe field or laboratory complex resistivity measurements. These models usually involve parameters known as chargeability and characteristic relaxation time. Empirical models such as the Pelton Cole-Cole resistivity model (Pelton et al., 1978) and the Debye decomposition approach (Nordsiek and Weller, 2008) were proposed to parameterize the SIP response. Other models are derived from equivalent circuits (see Dias (2000)). Chargeability and relaxation time are also involved in mechanistic models that describe the polarization effect observed when rocks are subjected to alternating electrical fields. The models of Wong (1979), Revil et al. (2015) and Misra et al. (2016a, 2016b) describe the polarization of metallic grains disseminated in a rock's pore space. Mechanistic models have also been proposed to explain the polarization of rocks in the absence of metallic minerals (Vinegar and Waxman, 1984; Revil and Florsch, 2010; Revil et al., 2012). SIP models can be validated using synthetic samples with well-known physical properties (e.g. Leroy et al.,2008; Gurin et al., 2015).

Experimental evidence shows that there is a strong relationship between the magnitude of electrical polarization and the surface-area to pore volume ratio (S_{por}), as first described by Börner and Schön (1991). Additional data then strengthened this relationship (Slater et al., 2006; Kruschwitz et al., 2010) and it was shown by Weller et al. (2010b) that values of chargeability can be used to infer S_{por}. A direct relationship between the Cole-Cole time constant and pore size has also been established (Kruschwitz et al., 2010; Niu and Revil, 2016). In the presence of metallic grains and without considering oxidation processes, it is the metallic grain size distribution that dictates the shape of the SIP responses of unconsolidated sands (Wong, 1979; Gurin et al., 2013, 2015). The approximations used in mechanistic models are not always representative

* Corresponding author.
E-mail addresses: cberube@ageophysics.com (C.L. Bérubé), michel.chouteau@polymtl.ca (M. Chouteau), pejman.shamsipour@polymtl.ca (P. Shamsipour), randy.enkin@canada.ca (R.J. Enkin), olivo@queensu.ca (G.R. Olivo).

http://dx.doi.org/10.1016/j.cageo.2017.05.001
Received 7 November 2016; Accepted 1 May 2017
Available online 03 May 2017

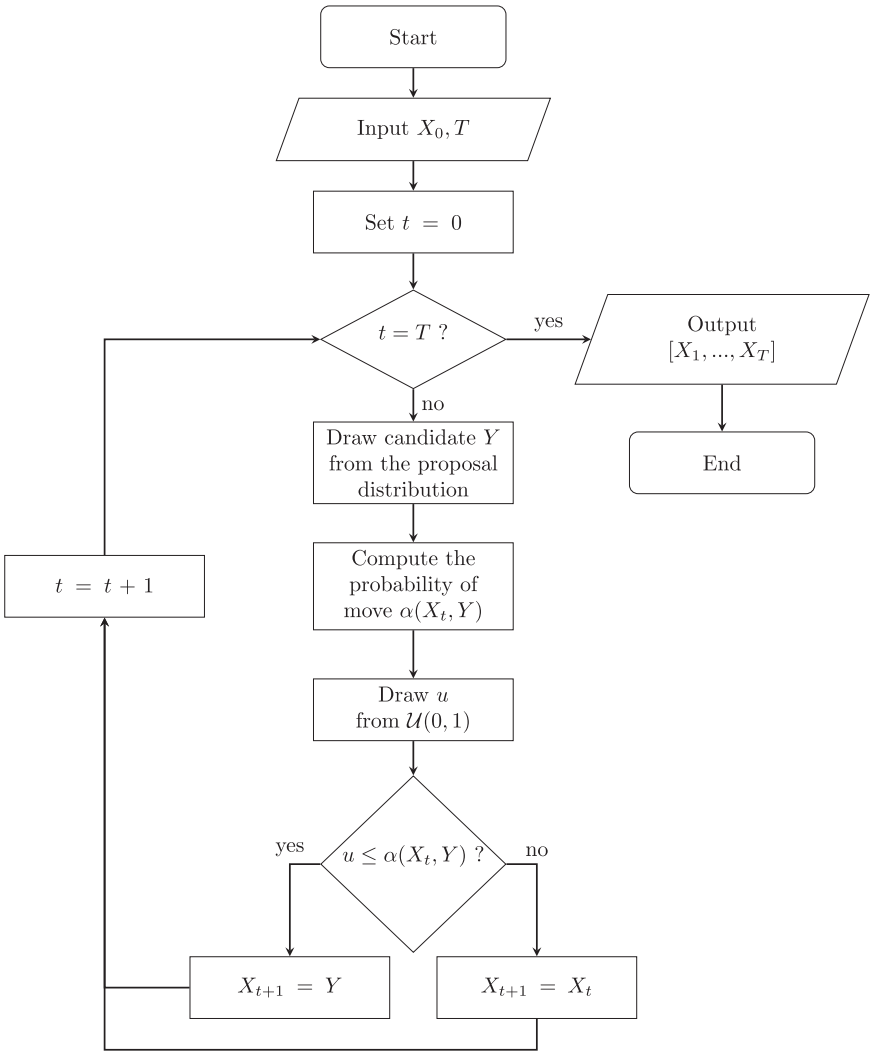

Fig. 1. Flowchart of the Metropolis-Hastings algorithm.

of real geological material. Extensive experimental data sets are needed to see if these models hold for more complex media such as the deformed and altered rocks that are often host to ore deposits. Studies that aim to characterize the SIP responses of rock samples from such deposits require fast and robust batch inversion codes.

In the SIP literature, three different approaches are often used to interpret SIP data. In the first, no curve fitting is required and only the basic features (peak value, frequency of the peak) of the imaginary part of conductivity are considered (e.g. Börner and Schön, 1991; Kruschwitz et al., 2010). The second approach consists of fitting the SIP data with a generalized Cole-Cole model or any of its variants. In this approach the optimization problem is overdetermined and fitting can be done using the nonlinear least squares formulation of Tarantola and Valette (1982). Lastly, interpretation of the SIP data can be done by performing a deconvolution of the complex resistivity spectra into a linear superposition of relaxations models. A Debye (Nordsiek and Weller, 2008) or Warburg (Revil et al., 2014) transfer function is typically used in the deconvolution scheme. In this approach, the problem is underdetermined and requires optimized regularization (Florsch et al., 2012, 2014).

Techniques based on the least-squares optimization have inconveniences. First, the inversion result is very dependent on the initial parameter estimation (e.g. Nordsiek and Weller (2008) and Weigand and Kemna (2016) for Debye decomposition). Batch inversion over large collections of laboratory measurements can prove to be a frustrating and time-consuming process for this reason. Second, they do not allow a straightforward estimation of the uncertainty around the recovered parameters. These two problems can be avoided by using a more global optimization approach such as a Markov-chain Monte Carlo (MCMC) simulation. With MCMC algorithms, the influence of the starting values diminishes as the simulation progresses. They also allow the propagation of measurement uncertainties during the inversion process. SIP parameter uncertainty is often neglected while attempts are made to establish relationships between SIP responses and rock properties (e.g. Zisser et al., 2010; Placencia-Gomez et al., 2013).

We developed BISIP, an open-source Python program to perform fast **B**ayesian **I**nversion of **S**pectral **I**nduced **P**olarization data using either Debye or Warburg decomposition, the Cole-Cole model, or any other empirical model based on simple circuits. An adaptive MCMC algorithm is implemented in BISIP. This approach offers significant advantages in terms of computation time when inverting SIP data with the decomposition approach, by comparison with the non-adaptive routine proposed by Keery et al. (2012). In this paper, parameter analysis of double Cole-Cole and Warburg decomposition inversions of synthetic data contaminated with varying levels of noise and of real SIP data measured on mineralized rocks from the Canadian Malartic gold deposit.

2. Bayesian inference using MCMC

From a Bayesian point of view, all model parameters and data are random quantities. If X denotes a vector of random variables (e.g. a data set) and θ represents a vector of model parameters, then the probability distribution of the parameters given the random variables is

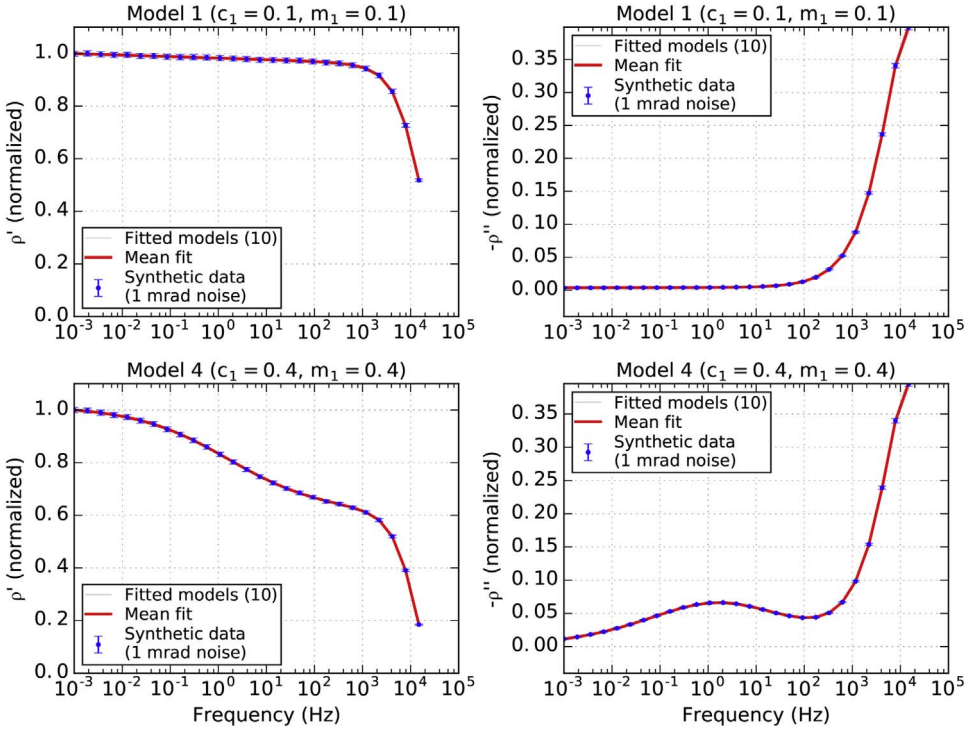

Fig. 2. Real and imaginary resistivity spectra of double Cole-Cole models 1 (a) and 4 (b) described in Table 1. Data is contaminated with errors of 1 mrad to simulate repetition of the measurements. The inversion is repeated 10 times, each time with new starting values draw randomly from the uniform priors. The mean fit is superimposed on the 10 inversion results.

Table 1
Parameters used for synthetic modelling of a double Cole-Cole type SIP spectra and the recovered parameters for different combinations of frequency dependence exponent and chargeability (c_1 and m_1, respectively). These parameters are never correctly recovered when the frequency exponent has a low value of 0.1. The correct parameters are recovered when the frequency dependence has a high value of 0.4.

	ρ_0 (Ω m)	m_1	c_1	τ_1 (s)	m_1	c_1	τ_2 (10^{-5} s)
Model 1 Synthetic	1000	0.1	0.1	0.1	0.9	0.9	1.0
($c_1 = 0.1$, $m_1 = 0.1$) Recovered	1039 ± 15	0.17 ± 0.03	0.06 ± 0.01	0.29 ± 0.01	0.89 ± 0.06	0.89 ± 0.01	0.96 ± 0.04
Model 2 Synthetic	1000	0.4	0.1	0.1	0.9	0.9	1.0
($c_1 = 0.1$, $m_1 = 0.4$) Recovered	929 ± 5	0.26 ± 0.01	0.17 ± 0.01	0.21 ± 0.02	0.96 ± 0.03	0.89 ± 0.01	1.03 ± 0.05
Model 3 Synthetic	1000	0.1	0.4	0.1	0.9	0.9	1.0
($c_1 = 0.4$, $m_1 = 0.1$) Recovered	1002 ± 3	0.100 ± 0.004	0.40 ± 0.02	0.122 ± 0.004	0.88 ± 0.06	0.90 ± 0.01	1.08 ± 0.04
Model 4 Synthetic	1000	0.4	0.4	0.1	0.9	0.9	1.0
($c_1 = 0.4$, $m_1 = 0.4$) Recovered	1001 ± 3	0.401 ± 0.004	0.40 ± 0.01	0.100 ± 0.002	0.85 ± 0.06	0.91 ± 0.01	1.04 ± 0.02

given by Bayes' theorem:

$$\pi(\theta \mid X) = \frac{p(X \mid \theta)p(\theta)}{\int p(X \mid \theta)p(\theta)d\theta}, \tag{1}$$

where $p(\theta)$ is the prior distribution of the parameters and $p(X|\theta)$ is a statistical model that reflects our understanding of the random variables given the model parameters. $\pi(\theta|X)$ is also known as the posterior distribution, and can be written as

$$\pi(\theta \mid X) = \frac{\mathcal{L}(\theta)p(\theta)}{c_n}, \tag{2}$$

where $\mathcal{L}(\theta)$ denotes the likelihood function and $c_n = \int p(X|\theta)p(\theta)d\theta$ is the normalization constant. The posterior distribution is therefore proportional to likelihood multiplied by the prior distribution. The goal of Bayesian inference is to obtain the posterior expectation of a function of θ or, more directly, of the parameters θ. The expected value of a function $f(X)$ can be obtained with Monte Carlo integration by drawing n random samples from the posterior distribution of X. The estimated expectation is

$$E[f(X)] \approx \frac{1}{n}\sum_{j=1}^{n} f(X_j). \tag{3}$$

The samples X_j can be drawn from the stationary distribution of a Markov chain. In the following sections, we describe two MCMC algorithms to produce such chains: the Metropolis-Hastings step method and an adaptive Metropolis step method.

2.1. Metropolis-Hastings algorithm

The Metropolis-Hastings algorithm was initially proposed by Metropolis et al. (1953) and was later generalized by Hastings (1970). Both algorithms use Markov chains to perform Monte Carlo integration. A Markov chain is defined as a sequence of random samples where the probability of the next sample depends only on the current one, i.e.,

$$P(X_{t+1} \mid X_1, \ldots, X_t) = P(X_{t+1} \mid X_t). \tag{4}$$

Markov chains must satisfy three conditions to be ergodic. A chain must be irreducible, aperiodic, and have a unique stationary distribution (see Gilks et al. (1995) for details on the Ergodic theorem).

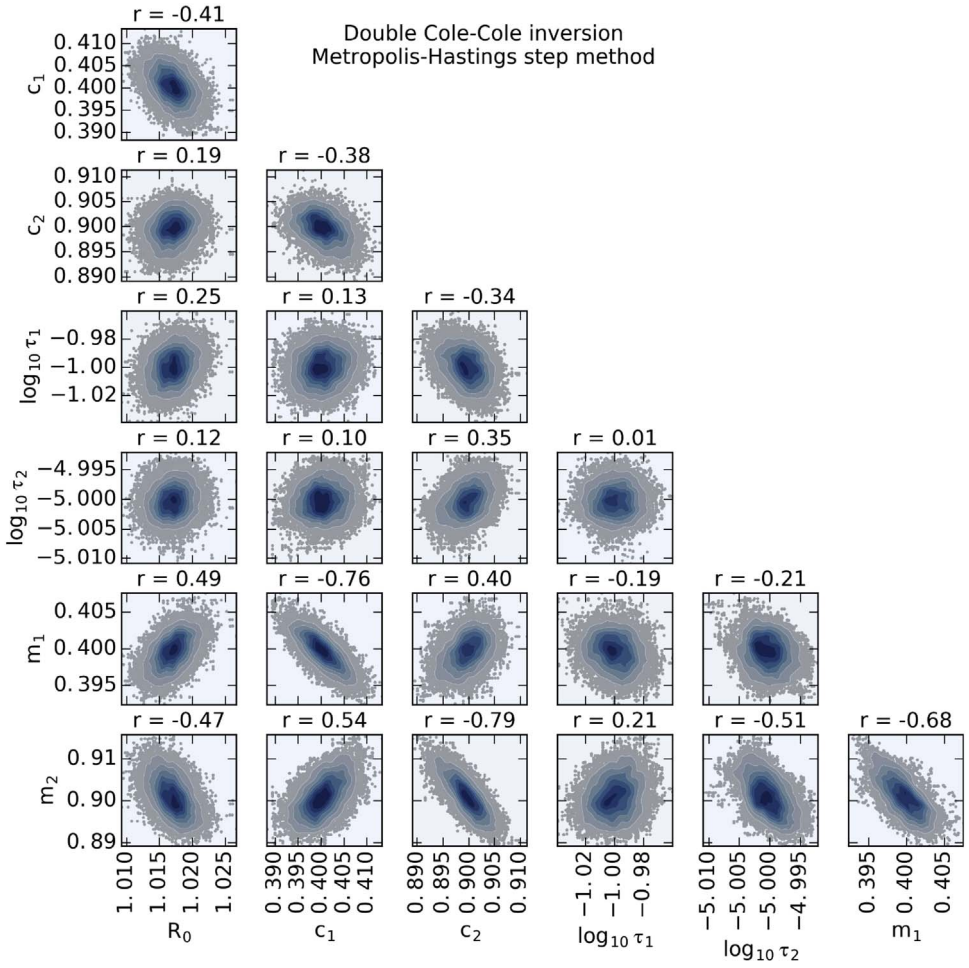

Fig. 3. Posterior distribution sampled from the stationary distribution after a double Cole-Cole inversion of synthetic data with well-defined imaginary resistivity peaks (model 4, Table 1). The results of 10 inversions with random starting values are superimposed. All 10 recovered models fit the data and the solution is unique.

The Metropolis-Hastings algorithm requires a starting value for the Markov chain (X_0). At every step of the chain, where the current value is X_t, a candidate sample Y is drawn from a proposal distribution, denoted by $q(X_t, Y)$. It must then be decided if the candidate Y will be accepted or rejected. If $\pi(\cdot)$ is the target distribution from which we wish to sample from after a large number of iterations (the posterior distribution), the probability of move α is defined by (Chib and Greenberg, 1995):

$$\alpha(X_t, Y) = \min\left[\frac{\pi(Y)q(Y, X_t)}{\pi(X_t)q(X_t, Y)}, 1\right] \tag{5}$$

Therefore, the chain always moves from X_t to the candidate Y if the ratio is greater than 1. If the ratio is lower than 1, the candidate is only accepted with probability $\alpha(X_t|Y)$. In the latter case, a random sample u is drawn from a uniform density between 0 and 1, denoted by $\mathcal{U}(0, 1)$. If $\alpha(X_t|Y)$ is greater than u, the candidate is accepted. Otherwise, it is rejected. An important special case is one where the proposal distribution is symmetric, resulting in $q(Y, X_t) = q(X_t, Y)$. If this condition is satisfied, the probability of move is reduced to the ratio between the posterior distributions. If the prior distributions are uniform, the probability of move further reduces to the likelihood ratio. The Metropolis-Hastings algorithm is summarized in Fig. 1, where T is the total number of iterations to perform.

Finally, the choice of proposal distribution has a strong influence on the convergence of the Markov chain toward the target stationary distribution (Roberts et al., 1997). We use the common choice of Gaussian proposal distribution centered on the current state of the chain. Acceptance rate is defined as the percentage of accepted samples during a segment of the Markov chain. Roberts et al. (1997) have shown that the optimal acceptance rate is 23.4% in high-dimensionality problems. In order to produce a Markov chain with good mixing, the acceptance rate is computed at user-defined intervals and the standard deviation of the proposal distribution is tuned accordingly (Roberts and Rosenthal, 2001).

2.2. Adaptive proposal distribution

Haario et al. (1999, 2001) first proposed the use of an adaptive proposal distribution in MCMC. A self-tuning proposal distribution allows to: (1) reduce the computational cost of tuning the proposal distribution scale to adjust the acceptance rate, and (2) reduce the amount of burn-in required when parameters are highly correlated.

In the adaptive algorithm, the stochastic variables are updated as a single block. Candidates are drawn from a multivariate normal distribution whose covariance depends on previous states. During burn-in, an initial delay period is used to gather information about the parameter space. After this delay an empirical covariance matrix is computed from the trace acquired so far. Then, the covariance is updated automatically at user-defined intervals. The adaptive Metropolis algorithm does not respect Eq. (4), and is therefore considered non-Markovian. However, work by Roberts and Rosenthal (2007) has shown that the adaptive Metropolis algorithm satisfies the Ergodic theorem if tuning of the covariance matrix is stopped after burn-in.

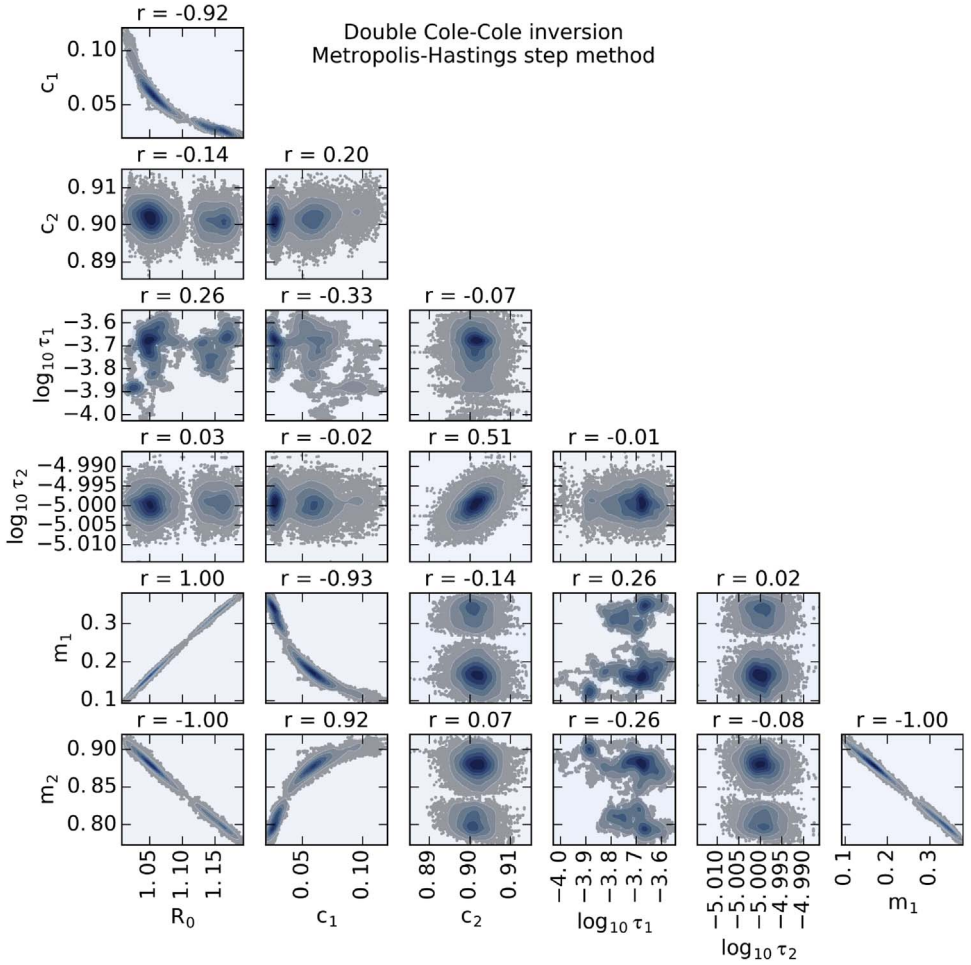

Fig. 4. Posterior distribution sampled from the stationary distribution after a double Cole-Cole inversion of synthetic data with $c_1 = 0.1$ (model 1, Table 1). The results of 10 inversions with random starting values are superimposed. All 10 recovered models fit the data but two solutions have been found for R_0, m_1, m_2 and c_1. The chain of τ_1 is also unstable.

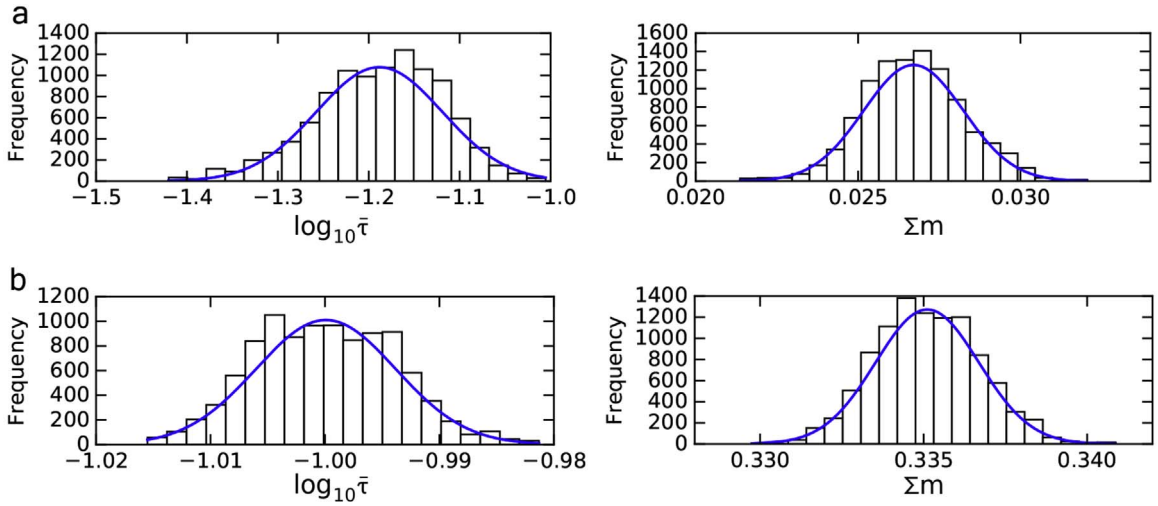

Fig. 5. Parameter histograms fitted with Gaussian distributions for the mean logarithmic relaxation time and total chargeability parameters after Debye decomposition of models 1 and 4 (a: m_1=0.1 and c_1=0.1, b: m_1=0.4 and c_1=0.4). 10 000 samples were drawn from the stationary distribution at the end of a 100 000 iterations Markov chain. Both integrating parameters have a unimodal posterior distribution, regardless of the shape of the SIP spectra.

3. Implementing MCMC for SIP inversion

In this section we describe how to implement MCMC techniques to estimate the SIP parameters of the generalized Cole-Cole model and the Debye or Warburg decomposition models. The likelihood function and the SIP transfer functions are first described. We then give the necessary parameter transformations and discuss the prior distributions for each model. Finally, we make practical recommendations on how to assess

Table 2
Parameter values used to generate synthetic data from a triple Cole-Cole model.

Synthetic triple Cole-Cole model		
DC resistivity	ρ_0 (Ω·m)	1000
Grain size	m_1	0.20
	c_1	0.40
	τ_1 (s)	10^3
Grain roughness	m_2	0.30
	c_2	0.35
	τ_2 (s)	10^{-2}
Maxwell-Wagner	m_3	0.40
	c_3	0.50
	τ_3 (s)	10^{-6}

convergence of the stochastic inversion.

3.1. Likelihood function

Complex resistivity (ρ^*) can be expressed in terms of real (ρ') and imaginary (ρ'') parts: $\rho^* = \rho' + i\rho''$, where $i^2 = -1$. The probability of measuring ρ^* given a set of SIP parameter (θ) is denoted by $P(\rho^*|\theta)$. If we make the assumption that the complex resistivity measurements follow a Gaussian distribution with mean μ and width σ (Ghorbani et al., 2007), the conditional probability of measuring ρ^* is given by

$$P(\rho^* \mid \mu, \sigma) = \frac{1}{\sqrt{2\pi}\sigma} \exp\left[-\frac{1}{2\sigma^2}(\rho^* - \mu)^2\right]. \tag{6}$$

For a series of N measurements through the range of frequencies that yield a set of ρ_i^* and their associated uncertainties σ_i^*, the likelihood $\mathcal{L}$ of measuring ρ^* is defined as the product of the probabilities of each measurement such that

$$\mathcal{L}(\rho^* \mid \mu, \sigma) = \prod_{i=1}^{N} P(\rho_i^* \mid \mu_i, \sigma_i^*). \tag{7}$$

In the inverse problem the measurements ρ_i^* and their uncertainties σ_i^* are known, and the goal is to estimate the mean of a distribution that fits the data using forward modelling. We define $\widehat{\rho_i^*}$ as the modelled complex resistivity, a function of the set of SIP parameters θ. Combining Eqs. (6) and (7) the likelihood of the model (and therefore the SIP parameters) becomes

$$\mathcal{L}(\theta \mid \rho^*, \sigma^*) = \prod_{i=1}^{N} \frac{1}{\sqrt{2\pi}\sigma_i^*} \exp\left[-\frac{1}{2\sigma_i^{*2}}(\rho_i^* - \widehat{\rho_i^*})^2\right]. \tag{8}$$

It should be noted that computing the log-likelihood is preferable (see Patil et al. (2010)), and that ρ^*, $\widehat{\rho^*}$ and σ^* can be defined as two-dimensional arrays containing the real and imaginary parts of resistivity. Chen et al. (2012) mention that it is possible to fit only the imaginary part of resistivity and including the real part in the objective function can cause bad results. The model must satisfy Kramers-Kronig relations. Therefore, if the model is not able to accurately fit both the real and imaginary part of the data, it implies that the uncertainty of the measurements was largely underestimated.

3.2. Generalized Cole-Cole model

The Cole-Cole resistivity and conductivity models have been used

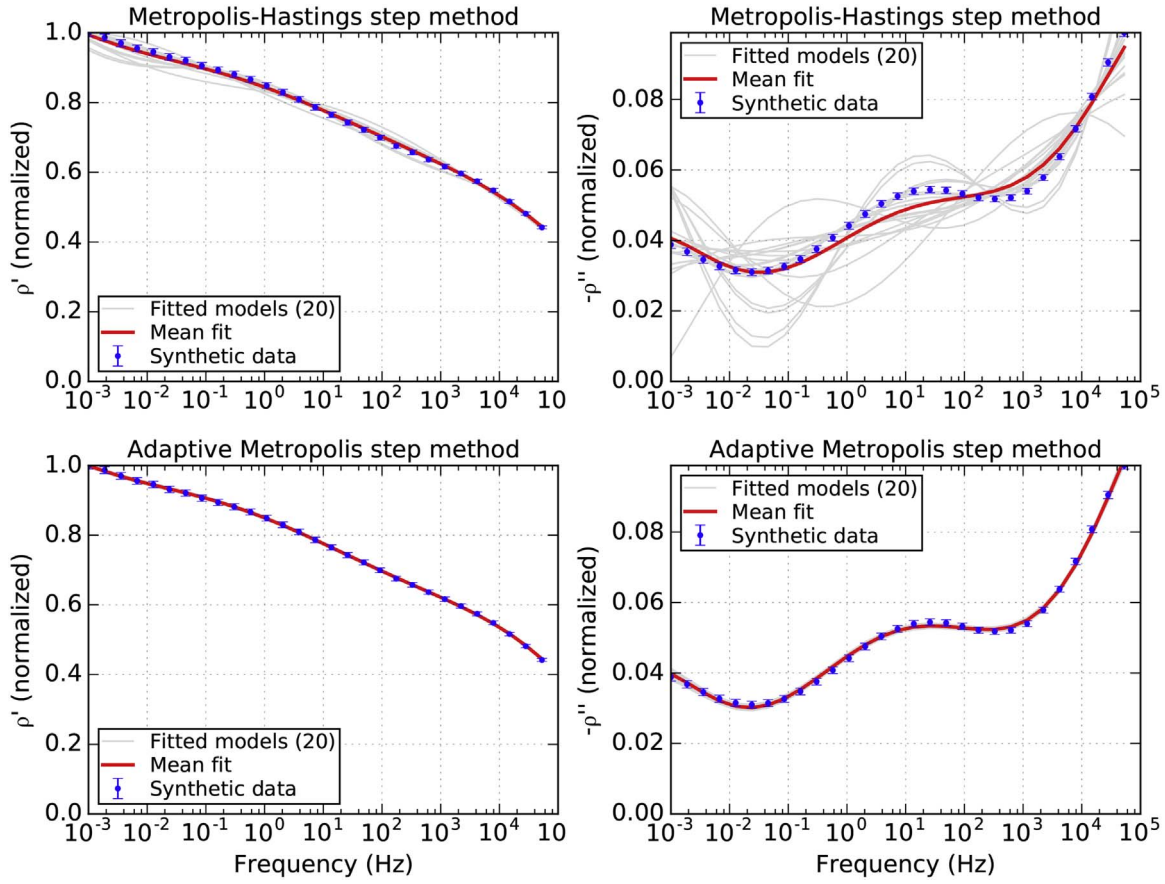

Fig. 6. Triple Cole-Cole synthetic data set fitted with a Warburg decomposition model using the adaptive and non-adaptive Metropolis step methods. The fitted models are obtained by running 20 independent Markov-chains with random starting values for all parameters. In each case the simulation is stopped after 600 000 iterations and the last 100 000 iterations are used to determine the optimal parameters (burn-in period of 500 000 iterations).

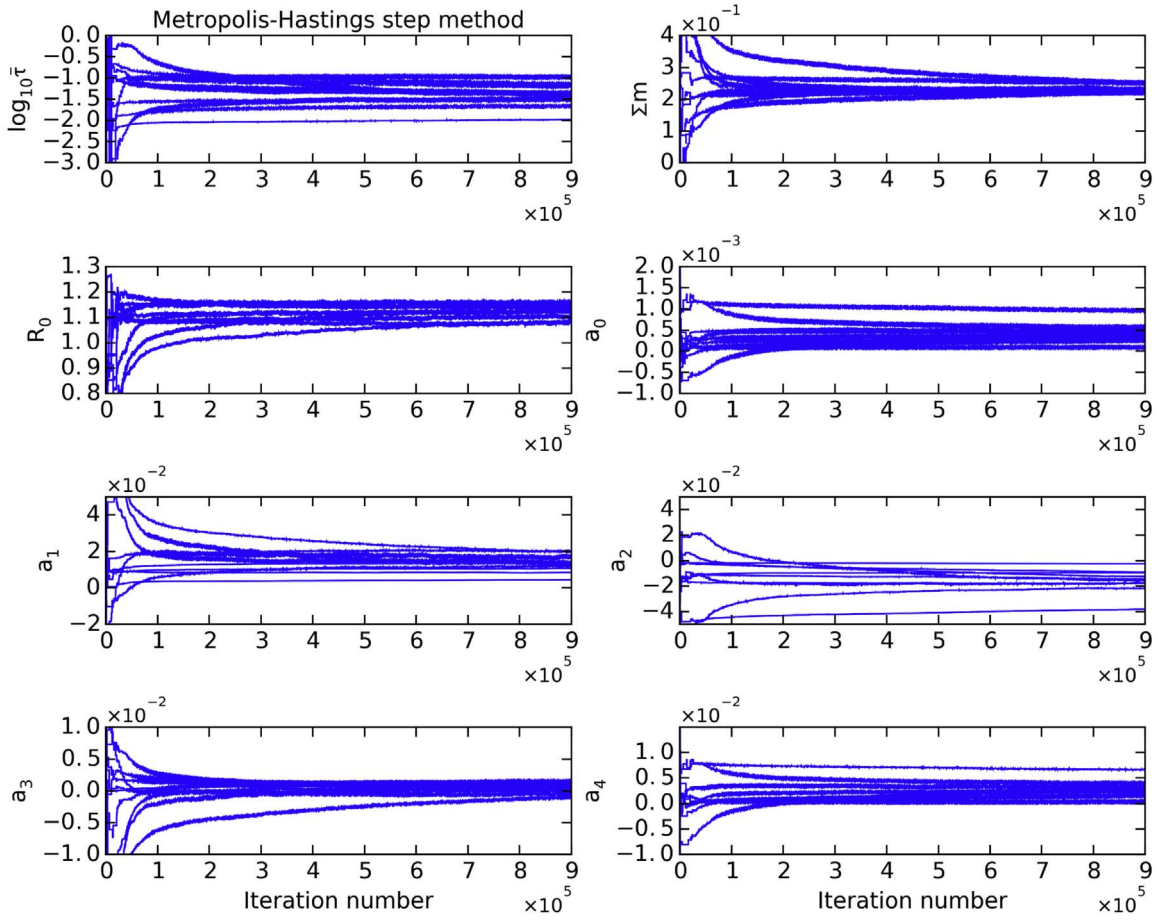

Fig. 7. Parameter traces of 10 attempts to fit the triple Cole-Cole type SIP spectra with a Warburg decomposition scheme using the Metropolis-Hastings step method. Each parameter is assigned a random starting value. The parameter traces reveal that the chains are slowly converging toward the same values but more iterations are needed for them to reach the stationary distribution.

extensively for the interpretation of SIP data in mineral exploration (Pelton et al., 1978; Vanhala and Peltoniemi, 1992), in environmental sciences (Vanhala, 1997; Placencia-Gomez et al., 2013, 2015) and to study the texture of porous materials (e.g. Binley et al., 2005; Kruschwitz et al., 2010). It may also be employed to extract spectral information from field time-domain induced polarization data (Johnson, 1984; Fiandaca et al., 2012). As mentioned in Tarasov and Titov (2013) (also see comments by Macnae (2013)), there are fundamental differences between the Cole-Cole resistivity and conductivity models. For laboratory measurements, a double or triple Cole-Cole model is typically used to fit the low, intermediate, and high-frequency parts of the spectra (see Fig. 13 of Leroy et al. (2008) for the physical meaning of each relaxation mode). The complex resistivity given by the generalized Cole-Cole model (Chen et al., 2008) is

$$\rho^*_{CC}(\omega) = \rho_0\left(1 - \sum_{l=1}^{L} m_l\left(1 - \frac{1}{1 + (i\omega\tau_l)^{c_l}}\right)\right), \tag{9}$$

where ω is the angular frequency ($\omega = 2\pi f$), ρ_0 is the DC resistivity and m_l, τ_l, and c_l are respectively the chargeability, relaxation time and frequency dependence exponent of the l^{th} relaxation mode. L may take values of 1, 2, 3 or more depending on the modality of the complex resistivity spectra. Adding more modes will quickly result in the inversion problem becoming underdetermined.

3.3. Debye and Warburg decomposition

The Debye decomposition approach has received increasing attention in recent SIP studies to infer grain or pore size distributions (e.g. Weller et al., 2010a, 2010b; Zisser et al., 2010; Gurin et al., 2013; Placencia-Gomez et al., 2013; Placencia-Gomez et al., 2015). The notion that complex conductivity can be interpreted as a sum of relaxation processes is based on the work of Morgan and Lesmes (1994) and Lesmes and Morgan (2001). The complex resistivity given by the Debye decomposition model is

$$\rho^*_{DD}(\omega) = \rho_0\left(1 - \sum_{k=1}^{K} m_k\left(1 - \frac{1}{1 + i\omega\tau_k}\right)\right), \tag{10}$$

and the complex resistivity given by the Warburg decomposition model is

$$\rho^*_{WD}(\omega) = \rho_0\left(1 - \sum_{k=1}^{K} m_k\left(1 - \frac{1}{1 + (i\omega\tau_k)^{1/2}}\right)\right). \tag{11}$$

where m_k and τ_k are respectively the chargeability and characteristic relaxation time parameters that correspond to each of the K superposed relaxation modes that form the relaxation time distribution (RTD). The Debye decomposition model corresponds to a Cole-Cole model with frequency dependence exponent value of c=1.0. Revil et al. (2014) have, however, recently shown that rocks and soils rarely produce a SIP response with frequency dependence above 0.5. Nordsiek and Weller (2008) and Zisser et al. (2010) have proposed deterministic methods to fit the Debye decomposition model to complex resistivity spectra using the linear least-squares formulation and a vector of predetermined relaxation times (K=1000 in the case of Zisser et al. (2010)). Integrating parameters such as total chargeability (Σm, the sum of all m_k chargeabilities) and mean relaxation time ($\bar{\tau}$, the logarithmic average value of all τ_k relaxation times weighted by their

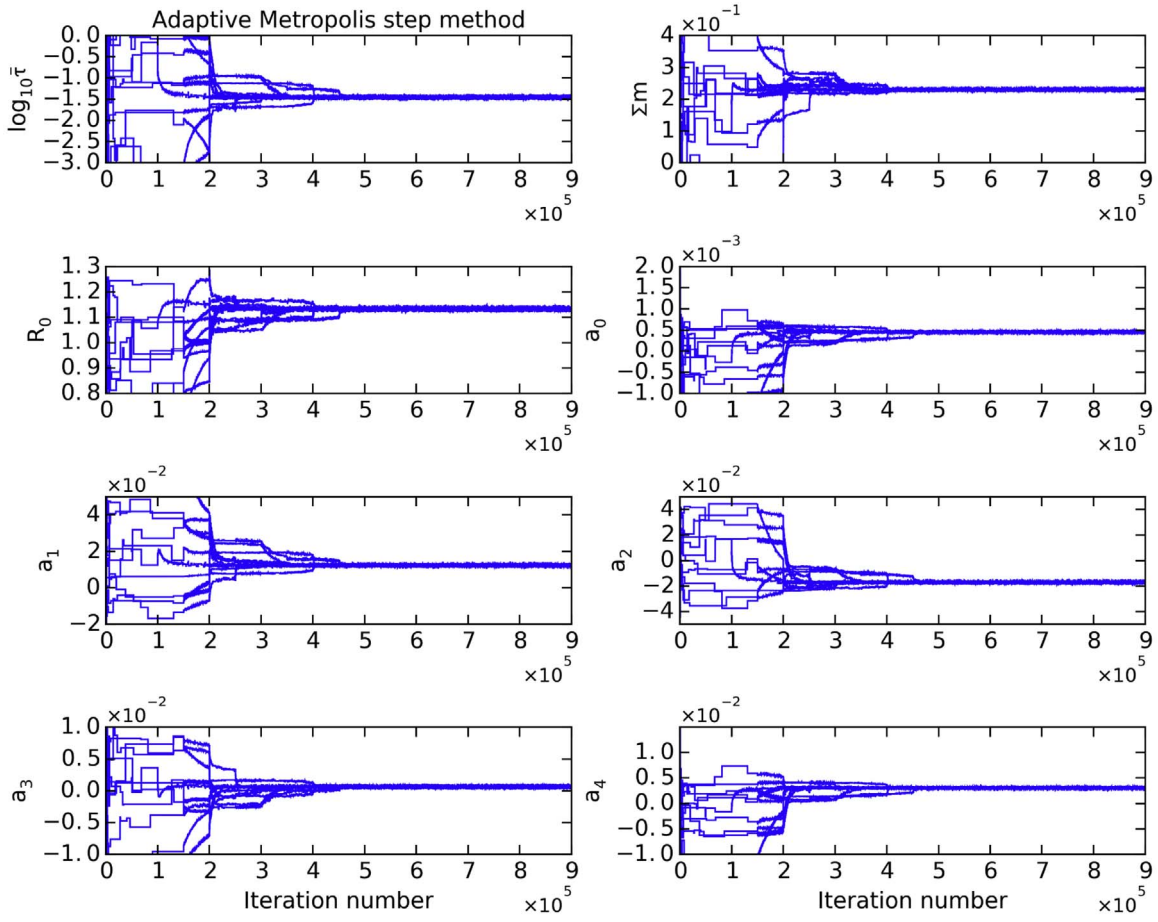

Fig. 8. Parameter traces of 10 attempts to fit the triple Cole-Cole type SIP spectra using the adaptive Metropolis step method and a Warburg decomposition scheme. Each parameter is assigned a random starting value. The traces of all parameters converge to the same stable value after 500 000 iterations.

corresponding chargeability) are derived from the RTD to simplify the results (see Nordsiek and Weller (2008)).

To perform Bayesian inference of the RTD in practical computation times, it is necessary to reduce the dimensionality of the decomposition scheme. Chargeability can be expressed as a polynomial function of relaxation time (Keery et al., 2012). The generalized equation for a polynomial RTD is

$$m(\tau) = \sum_{p=0}^{P} a_p (\log_{10}\tau)^p , \tag{12}$$

where P is the order of the polynomial approximation, and a_p are the polynomial coefficients. The parameters to estimate are therefore the polynomial coefficients a_0 to a_P and the DC resistivity ρ_0. The fourth-order approximation used by Keery et al. (2012) is not always necessary and sometimes result in superfluous parameters, preventing the simulation from converging. Higher order approximations may also be needed to fit highly multimodal SIP spectra. Finally, it is evident from Fig. 6b of Keery et al. (2012) that the regular Metropolis-Hastings algorithm struggles in the parameter space of a Debye decomposition and that the chains of the polynomial coefficients can be unstable.

3.4. Prior distributions

Although the MCMC sampling process becomes independent of the starting values after the chain has reached the stationary distribution, initial guesses for the parameters are still required to launch the simulation. A practical approach is to launch several chains using dispersed starting values drawn from regions of high posterior density (Gelman and Rubin, 1992), or simply use several different starting values drawn from uniform prior distributions.

3.4.1. Cole-Cole parameters

Uniform prior distributions are used for the Cole-Cole parameters. Prior information includes lower and upper bounds of the prior distributions, which are selected based on the physical meaning of the parameter (e.g. $0 \leq m \leq 1$ for chargeability and $0 \leq c \leq 1$ for frequency dependence). The relaxation time parameter is strictly positive and may vary over several orders of magnitude. Therefore, this parameter is log-transformed and the bounds of the uniform prior distribution that describe it are set to include values typically found in the literature (e.g. $-6 \leq \log_{10}\tau \leq 3$).

3.4.2. Decomposition parameters

Uniform prior distributions are assigned to the polynomial coefficients for the decomposition approach. We found that an interval of $[-0.1, 0.1]$ generally contains values of the polynomial coefficients that describe a typical RTD. The polynomial coefficients often switch between negative and positive values. A reasonable hypothesis is that the polynomial coefficients can be described by a normal prior distribution, centered on 0. More extensive collections of inversion results with the stochastic decomposition approach are however needed to confirm this hypothesis.

3.5. Convergence of the chains

Raftery and Lewis (1992) have proposed a quantitative convergence diagnostic to determine the amount of iterations and burn-in required for a single long Markov chain. The burn-in period refers to the initial

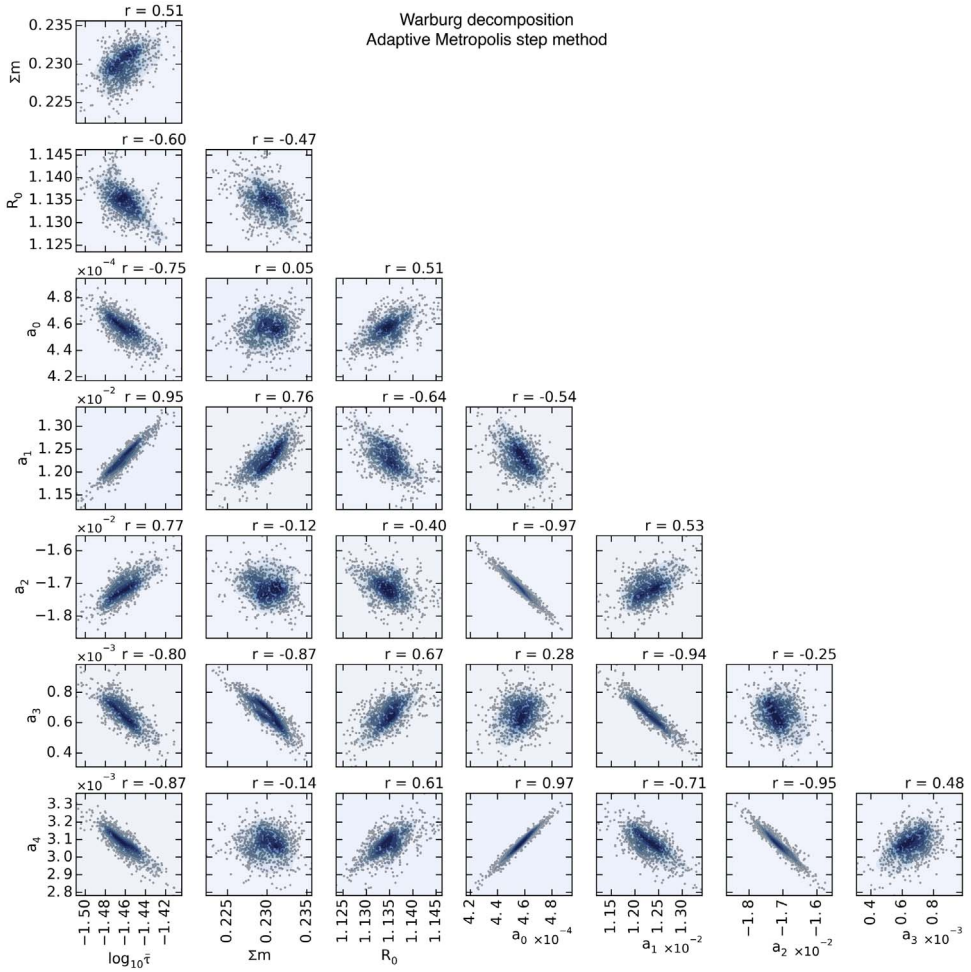

Fig. 9. Posterior distribution of a Warburg decomposition of the synthetic triple Cole-Cole SIP data. During the burn-in period the adaptive Metropolis algorithm was used. Scatter points correspond to the [500 000 – 600 000] interval in Fig. 8. Biplots reveal strong correlation between the polynomial coefficients, especially between a_0 and a_2, a_0 and a_4, a_1 and a_3, and a_2 and a_4. Total chargeability (Σm) and mean relaxation time ($\bar{\tau}$) are deterministic variables.

iterations required to reach the stationary state. For a single chain, however, it is unknown if the chain has explored all regions of the posterior distribution (Brooks, 1998). It can be argued that convergence is only truly reached when multiple chains with dispersed initial values have been shown to converge toward the same stationary distribution. Gelman and Rubin (1992) have developed a convergence diagnostic that consists of running multiple chains with dispersed starting values and comparing the estimated between-chains and within-chain variances for each parameters. A comprehensive review of MCMC convergence diagnostics is available in Cowles and Carlin (1996).

4. Results and discussion

Synthetic SIP data sets were generated using double and triple Cole-Cole models with varying relaxation times, frequency dependence and chargeability values. In this section, we first test our stochastic inversion program to assess the convergence and parameter recovery of the algorithm. Important limitations regarding the capability of double Cole-Cole models to recover the correct parameters in particular cases are highlighted. Then, the Debye and Warburg decomposition approaches are tested on the synthetic spectra for which the Cole-Cole parameters were not recovered. Next, a comparison between the Metropolis-Hastings and adaptive Metropolis step methods for the estimation of Warburg or Debye RTD is presented, followed by an analysis of the impact of phase measurement noise on the recovered RTD. Finally, BISIP is tested on real SIP data measured on mineralized rocks from the Canadian Malartic gold deposit.

4.1. MCMC inversion using the Cole-Cole model

Synthetic double Cole-Cole models with varying chargeability and frequency dependence exponents are fitted using the Metropolis-Hastings step method (Fig. 2). The parameter values used to generate the synthetic SIP responses and the parameter values recovered from inversion of four models are summarized in Table 1. For low c_1 values (models 1 and 2), all parameters that describe the low-frequency relaxation (R_0, c_1, m_1, τ_1), are not correctly recovered whereas the parameters that describe the high-frequency relaxation (c_2, m_2, τ_2) are recovered within an acceptable range. For high values of c_1 (models 3 and 4), all parameters are correctly recovered, with the most accurate results being obtained when both c_1 and m_1 are equal to 0.4.

The inversion process is repeated 10 times with different initial values drawn from the prior distributions. Bivariate analysis of the parameter traces confirms that the solution to the double Cole-Cole inversion is unique when both peaks are well-defined (Fig. 3). In such a case, all parameters take on a Gaussian posterior density. On the other hand, the MCMC simulation is unstable when the c exponent of one of the Cole-Cole modes is near 0.1. Fig. 4 shows the posterior distribution of this particular case, also after performing 10 inversions using random initial values. The 10 inversions yield indiscernible fits on Fig. 2. However, the R_0, c_1, m_1 and m_2 parameters have a bimodal posterior distribution. Possible values of the chargeability parameter m_1 vary in a range between 0.10 and 0.40 whereas the frequency dependence parameter c_1 varies in a range between 0 and 0.15. The strong correlation (Pearson r=−0.93) between these two parameters

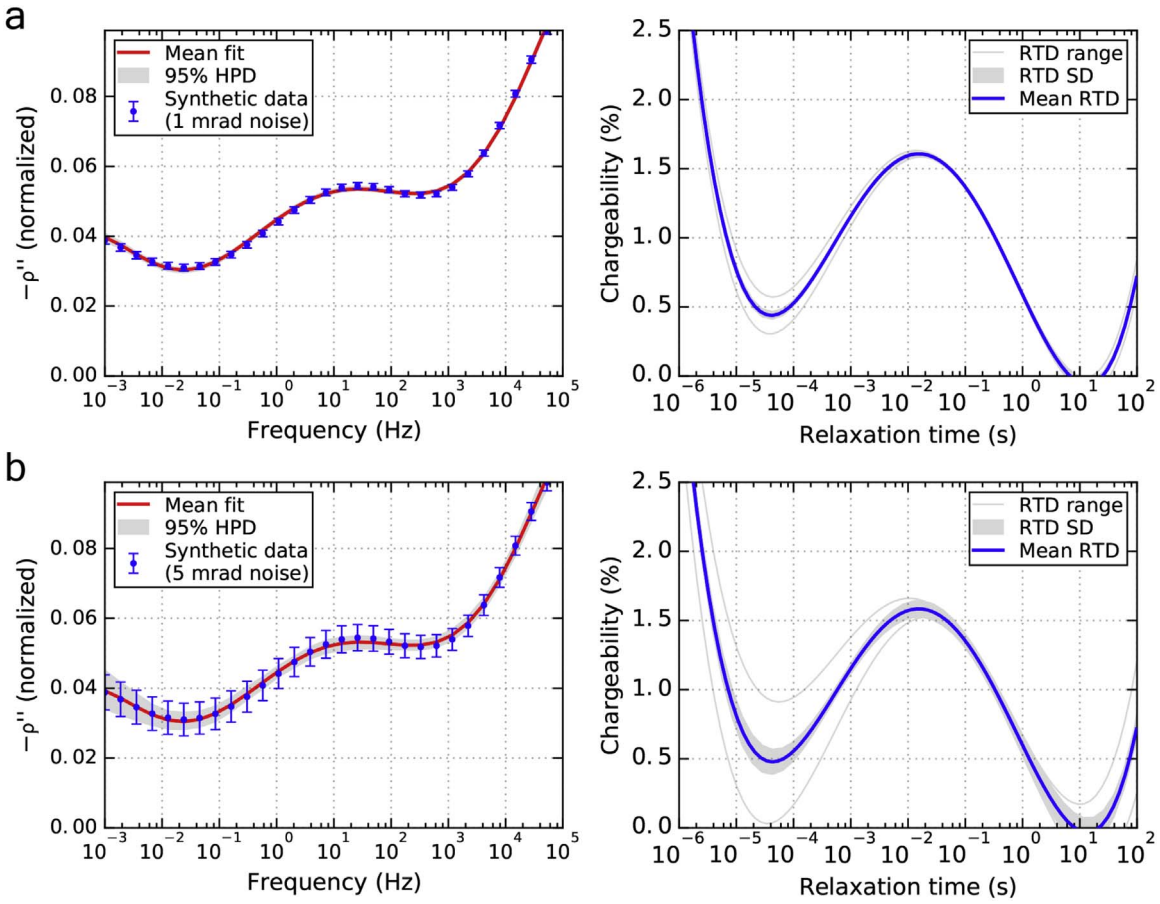

Fig. 10. The impact of phase measurement noise on the estimation of the RTD. The synthetic data is contaminated with noise levels of 1 mrad (a) and 5 mrad (b). The mean fit and the 95% highest posterior density interval are drawn over the synthetic data on the left. The estimated Warburg RTD, its range and its standard deviation are drawn on the right.

implies that small increments of the m_1 parameter are easily compensated by small decrements of the c_1 parameter without affecting the likelihood. Consequently, the flat shape of the phase shift spectra in the low-frequency range may be fitted by either low c_1 exponent and chargeability (the expected result) or by a lower value of c_1 paired with a high enough value of chargeability (m_1) to make the curve look flat at the scale of the data range. It is worth noting that the parameter space is diagonal (Pearson r=1.00) between the R_0 and m_1 parameters, the R_0 and m_2 parameters, and the m_1 and m_2 parameters, and that it is "banana-shaped" between R_0 and c_1, c_1 and m_1, and c_1 and m_2.

4.2. Adaptive MCMC inversion with the decomposition scheme

The decomposition approach provides an alternative for fitting SIP data when relaxation peaks are not well defined in the data. In this section we show that the Metropolis-Hastings algorithm performs well with the Debye or Warburg decomposition schemes when a third order polynomial approximation of the RTD is used. However, the Metropolis-Hastings step method is unable to converge in reasonable computation times for more multimodal SIP spectra requiring fourth or fifth order polynomial approximations. The latter is also very dependent on starting values. We now show that the adaptive Metropolis step method implemented in BISIP performs better than the non-adaptive option in the highly correlated parameter space of a Warburg decomposition.

4.2.1. Third order Debye decomposition

The spectra of models 1 and 4 (Table 1) generated in the previous section were fitted using the Debye decomposition scheme and the Metropolis-Hastings step method. The Debye decomposition approach was able to properly fit the synthetic Cole-Cole spectra regardless of the c_1 value used to generate them. In both cases a 3rd order polynomial approximation was used for the RTD. Then, integrating parameters of total chargeability and mean logarithmic relaxation time are computed from the RTD in a range from 0.001 to 10 s. To assess the stability of the recovered of the RTD, the traces of these two deterministic variables are plotted in histograms (Fig. 5). Contrary to the double Cole-Cole inversion, the SIP parameters recovered using the Debye decomposition scheme are unique and the MCMC algorithm has reached a stable solution.

4.2.2. Fourth order Warburg decomposition

A synthetic data set representative of a highly multimodal SIP spectra was generated using a triple Cole-Cole model. The synthetic SIP spectra features three distinct modes: (1) a partly defined low-frequency (<0.1 Hz) mode describing the grain size distribution, (2) a well-defined intermediate frequency (1–100 Hz) phase peak representative of grain roughness, and (3) a high-frequency (>1 kHz) feature for Maxwell-Wagner polarization (see Fig. 13 of Leroy et al., 2008). The synthetic data is contaminated with phase shift errors of 1 mrad and amplitude errors of 0.1%. Table 2 summarizes the values used to generate the synthetic triple Cole-Cole data.

This multimodal SIP data set is fitted with a fourth order Warburg decomposition approach, first using the Metropolis-Hastings step method as implemented in Keery et al. (2012), and next using our adaptive Metropolis step method. To compare the performance of both step methods, we launch 20 independent Markov-chains of 600 000 iterations with a burn-in period of 500 000 iterations. In the adaptive MCMC algorithm, the first covariance matrix is computed after an initial 50 000 iterations. It is then updated every 50 000 iterations and fixed after the burn-in period. For each chain, new starting values of all

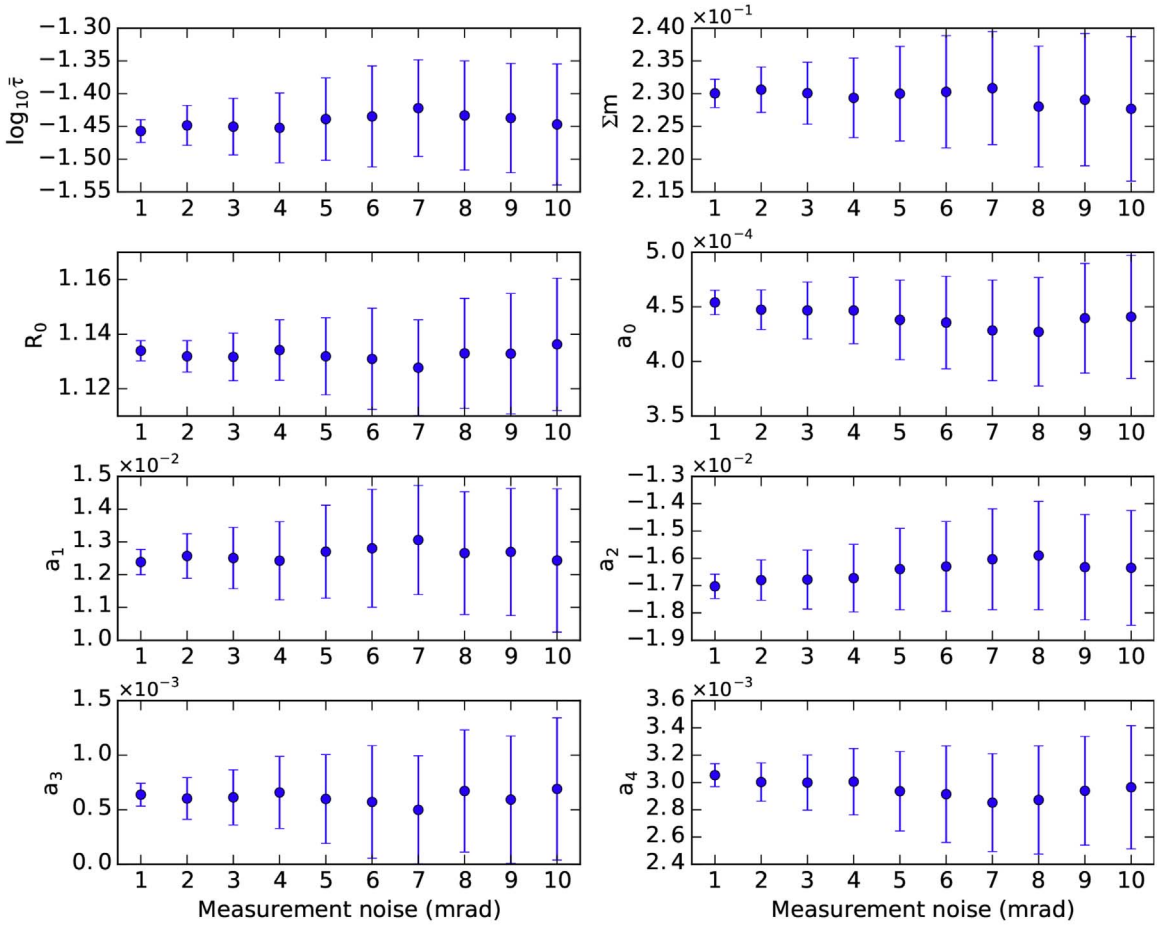

Fig. 11. Inferred Warburg decomposition parameters of a synthetic triple Cole-Cole data set for phase measurement noise levels ranging from 1 to 10 mrad.

Table 3
Sulfur content associated with pyrite alteration, physical properties and recovered SIP parameters of two altered metagreywacke samples from the Canadian Malartic gold deposit. The two samples have the same mineral assemblage and mostly differ by their degree of pyrite alteration. The Cole-Cole parameters are undefined for sample A.

	Sample A	**Sample B**
Sulfur content (%)	0.095 ± 0.005	0.454 ± 0.005
Gold content (*ppm*)	0.01	0.1
Density (g/cm^3)	2.753 ± 0.003	2.788 ± 0.003
Porosity (%)	0.8 ± 0.1	1.3 ± 0.1
Magnetic susceptibility (*SI*)	(2.89 ± 0.12) × 10^{-4}	(3.00 ± 0.07) × 10^{-4}
Resistivity ($\Omega \cdot m$)	2800 ± 420	1571 ± 283
Cole-Cole c_1	–	0.46 ± 0.04
Cole-Cole m_1	–	0.15 ± 0.01
Cole-Cole τ_1 (s)	–	0.12 ± 0.01
Warburg $\sum m$	0.054 ± 0.002	0.15 ± 0.01
Warburg $\bar{\tau}$ (s)	0.34 ± 0.01	0.30 ± 0.01

parameters are randomly drawn from the prior distribution. The solutions obtained with both step methods are drawn in Fig. 6. With the Metropolis-Hastings step method, the mean of the 20 fitted models converges toward the data points. However only 1 of the fitted model passes through every data point. With the Adaptive Metropolis step method, all 20 Markov-chains have produced models that fit the data.

Warburg (and Debye) decomposition fitting of multimodal SIP spectra is highly dependent on the initial starting values when using the regular Metropolis-Hastings step method. Even if the independent Markov-chains converge, on average, toward a model that properly fits the data, most of the chains have not reached the stationary distribution at the 900 000 iterations mark (Fig. 7). By comparison, for equal-length chains, the dependence of the initial parameter values on the fitted models is diminished when using an adaptive step method that updates the RTD polynomial coefficients as a single block parameter. Fig. 8 shows the progression of 10 independent adaptive Metropolis chains, which all converged toward the same value after 500 000 iterations.

When comparing the traces in Figs. 7 and 8, it is apparent that the MCMC simulation progresses much slower with the Metropolis-Hastings step method than with the adaptive Metropolis step method. The slow convergence of the Markov-chains with the regular Metropolis-Hastings sampler is explained by: (1) the strong correlation between the polynomial coefficients that describe the Warburg RTD and (2) the existence of local high posterior density traps around the global maximum. The Pearson correlation coefficient is particularly high between the a_0 and a_2 parameters (r=−0.97), the a_0 and a_4 parameters (r=0.98), the a_1 and a_3 parameters (r=−0.93), and the a_2 and a_4 parameters (r=−0.96) (Fig. 9). This observation implies that at maximum likelihood (reached shortly after 400 000 iterations), small increments of a_0 are easily compensated by increments of a_4 and decrements of a_2, and so on.

4.3. Propagation of measurement noise on the RTD

One of the main advantages of using MCMC simulation to estimate the RTD of rock and soil samples is the ability to quantify the uncertainty around the inversion solution. In this section, we contam-

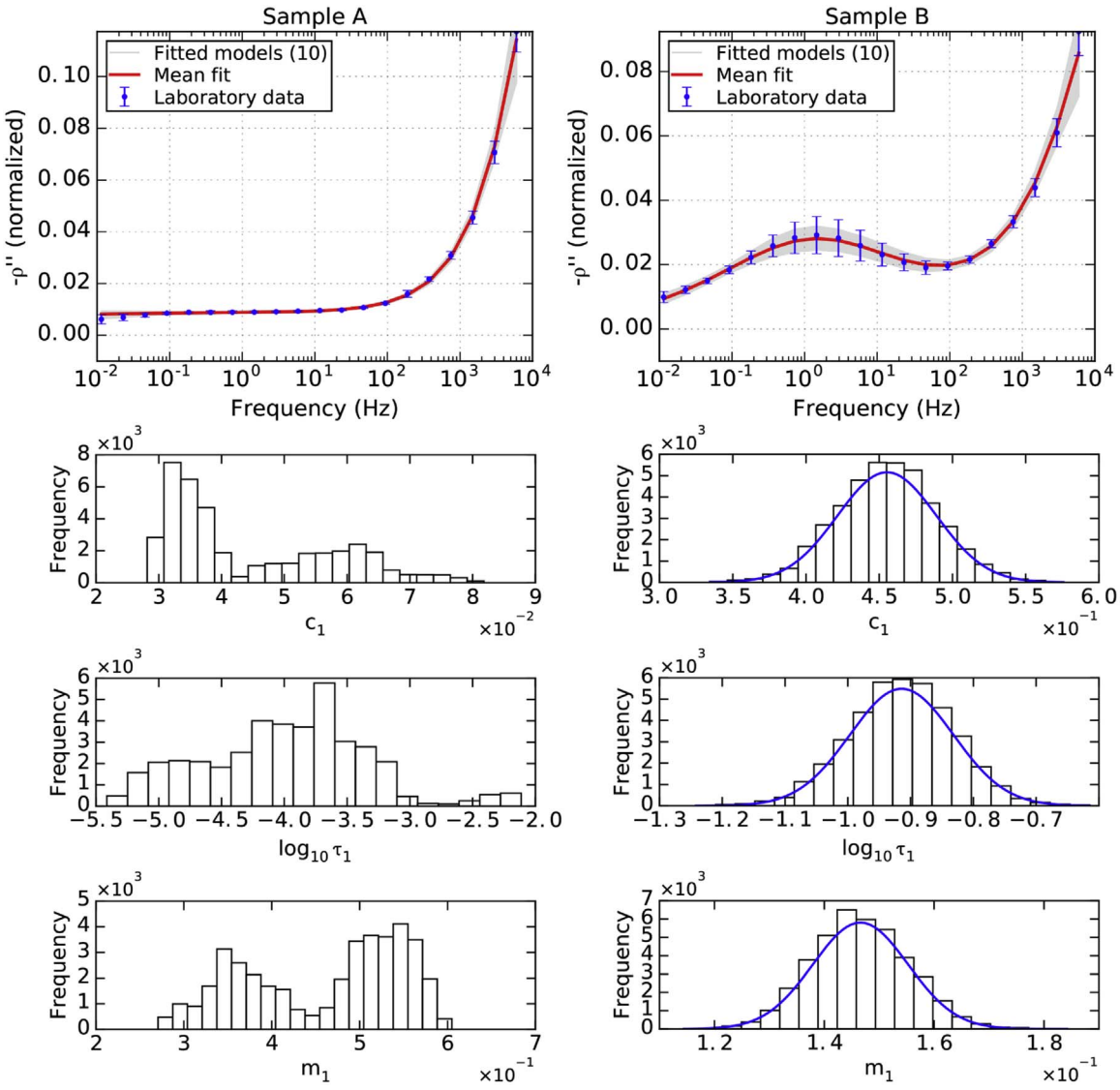

Fig. 12. Fitting results and parameter histograms after double Cole-Cole inversion of SIP laboratory measurements on two altered metagreywacke samples with sulfur contents of (0.095 ± 0.005)% (Sample A) and (0.454 ± 0.005)% (Sample B). The grey area around the fitted model represents the 95% highest posterior density interval at the end of the simulation. The 10 independent chains with random starting values produced identical fits but two solutions are found for c_1 and m_1 in the case of sample A. Results obtained with the Metropolis-Hastings step method.

inate the synthetic triple Cole-Cole spectra of Table 2 with varying amounts of noise 1–10 mrad) on the phase shift. Fig. 10 shows the estimated RTD and its uncertainty for noise levels of 1 and 5 mrad. There is a direct relationship between measurement error and the uncertainty of the estimated polynomial coefficients (Fig. 11). With typical laboratory errors (below 5 mrad) the solution remains well-defined. It can be argued that the error on the RTD is negligible for noise levels below 1 mrad. Above 5 mrad, the range of possible distributions become important, and several independent Markov-chains should be run and averaged.

4.4. Inversion of laboratory data

We tested BISIP on real SIP spectra measured on rock samples from the Canadian Malartic gold deposit, where gold occurs mainly as inclusions in pyrite which is hosted in Archean sedimentary rocks (Helt et al., 2014; Perrouty et al., 2017). The physical properties, SIP parameters, and sulfur content of both samples can be found in Table 3. Fig. 12 shows that mineralized greywacke samples produce phase shift peaks in the range of 0.1–10 Hz. The phase shift peak associated with sample B (containing up to 0.454% sulfur in the form of pyrite mineralization) reaches 30 mrad while the one measured on sample A (with only 0.095% sulfur) is limited to 10 mrad. In both cases, multiple Cole-Cole inversions points toward a model that passes through all data points. However, when the relaxation peak is not obvious (Fig. 12A), the parameter histograms show a bimodal tendency, with possible solutions of c_1 at 0.035 and 0.060, and possible solutions of m_1 at 0.35 and 0.55. In Fig. 12B, the phase shift curve resembles the synthetic spectra generated with high values of c_1, and the posterior distribution is unimodal Gaussian with mean values of $c_1 = 0.46 \pm 0.03$ and $m_1 = 0.15 \pm 0.01$.

We then launch 10 independent inversions with random starting values using Warburg decomposition and the adaptive Metropolis algorithm (Fig. 13). The traces of total chargeability and mean relaxation time have reached a stationary distribution and the inversion has a unique solution. Proper estimation of SIP parameters is vital to reduce the dimensionality of electrical properties of rocks in studies where large data sets of mineral exploration data from different disciplines are to be integrated in a common earth model. The MCMC inversion technique implemented in BISIP is well-suited for this type of problem. First, it facilitates batch inversion by minimizing the influence of user guesses. Second, analysis of the parameter traces

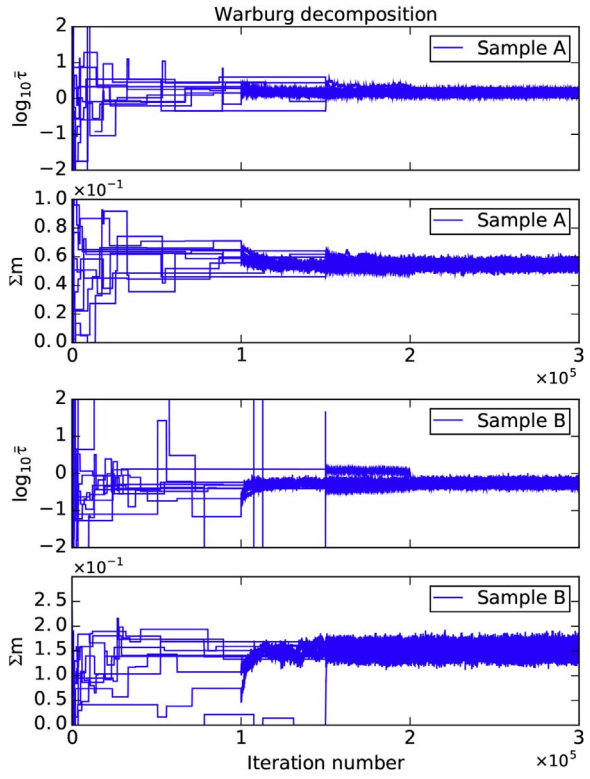

Fig. 13. Parameter traces of the mean relaxation time and total chargeability parameters after a third order Warburg decomposition of the SIP spectra measured on samples A and B. The 10 independent chains with random starting values converged toward the unique solution after 200 000 iterations regardless of the shape of the SIP spectra. Computation time was 35 s per chain using the adaptive Metropolis step method.

allow the user to accept or reject the inversion results before feeding them to a common earth model.

5. Conclusions

Batch inversion of laboratory rock complex resistivity data using the classic least squares approach can prove to be a tedious and frustrating process due to the high amount of user-interaction needed to fit SIP curves. This process requires even more user knowledge when the measurements are performed on weakly polarizable samples. The optimization algorithm implemented in BISIP reduces the influence of initial guesses and the amount of user-interaction required to fit SIP data, therefore making batch or time-lapse inversion of hundreds of laboratory measurements a simpler process.

It was shown in this paper that the Cole-Cole model should be avoided when fitting SIP curves produced by weakly polarizable samples. In this case, the solution to the inverse problem is not unique. The stochastic Debye or Warburg decomposition scheme has a unique solution regardless of the shape of the SIP spectra. However, inversion through the decomposition scheme progresses slowly when using the regular Metropolis-Hastings algorithm. This poor performance is explained by the strong correlation between several of the polynomial coefficients that describe the RTD. We have shown that our adaptive Metropolis step method performed better than its non-adaptive counterpart in the case of Warburg decomposition. Finally, the importance of properly estimating SIP parameter uncertainty before propagating them into mechanistic models was highlighted by showing the direct relationship between measurement uncertainty and the range of possible recovered RTD.

BISIP is available under the MIT open-source licence. We hope to provide the geophysics and petrophysics community with a base for further developments in stochastic inversion of laboratory SIP data and to make parameter analysis of SIP transfer functions a simpler process. The source code, standalone executables, and documentation of the program presented in this study are maintained at https://github.com/clberube/bisip.

Acknowledgements

We thank the subject matter experts and all our colleagues from the Canadian institutions involved in the CMIC Footprints project for valuable discussions. We thank A. Revil, the associate editor and the two anonymous reviewers for their constructive comments. Funding was provided by NSERC and CMIC through the NSERC CRD Program and by the FRQNT. CMIC-NSERC Exploration Footprints Network Contribution 110.

References

Börner, F.D., Schön, J.H., 1991. A Relation between the Quadrature Component of Electrical Conductivity and the Specific Surface Area of Sedimentary Rocks. Log. Anal. 32 (05).
Binley, A., Slater, L.D., Fukes, M., Cassiani, G., 2005. Relationship between spectral induced polarization and hydraulic properties of saturated and unsaturated sandstone. Water Resour. Res. 41 (12), W12417.
Brooks, S., 1998. Markov chain Monte Carlo method and its application. J. R. Stat. Soc.: Ser. D. (Stat.) 47 (1), 69–100.
Chen, J., Kemna, A., Hubbard, S.S., 2008. A comparison between Gauss-Newton and Markov-chain Monte Carlo-based methods for inverting spectral induced-polarization data for Cole-Cole parameters. Geophysics 73 (6), F247–F259.
Chen, J., Hubbard, S.S., Williams, K.H., Flores Orozco, A., Kemna, A., 2012. Estimating the spatiotemporal distribution of geochemical parameters associated with biostimulation using spectral induced polarization data and hierarchical Bayesian models. Water Resour. Res. 48 (5), W05555.
Chib, S., Greenberg, E., 1995. Understanding the Metropolis-Hastings Algorithm. Am. Stat. 49 (4), 327–335.
Cowles, M.K., Carlin, B.P., 1996. Markov Chain Monte Carlo Convergence diagnostics: a comparative review. J. Am. Stat. Assoc. 91 (434), 883–904.
Dias, C.A., 2000. Developments in a model to describe low-frequency electrical polarization of rocks. Geophysics 65 (2), 437–451.
Fiandaca, G., Ramm, J., Binley, A., Gazoty, A., Christiansen, A.V., Auken, E., 2012. Resolving spectral information from time domain induced polarization data through 2-D inversion. Geophys. J. Int., ggs060.
Florsch, N., Camerlynck, C., Revil, A., 2012. Direct estimation of the distribution of relaxation times from induced-polarization spectra using a Fourier transform analysis. Surf. Geophys. 10 (6), 517–531.
Florsch, N., Revil, A., Camerlynck, C., 2014. Inversion of generalized relaxation time distributions with optimized damping parameter. J. Appl. Geophys. 109, 119–132.
Gelman, A., Rubin, D.B., 1992. Inference from Iterative Simulation Using Multiple Sequences. Stat. Sci. 7 (4), 457–472.
Ghorbani, A., Camerlynck, C., Florsch, N., Cosenza, P., Revil, A., 2007. Bayesian inference of the Cole-Cole parameters from time- and frequency-domain induced polarization. Geophys. Prospect. 55 (4), 589–605.
Gilks, W.R., Richardson, S., Spiegelhalter, D., 1995. Markov Chain Monte Carlo in Practice. CRC Press Dec.
Gurin, G., Tarasov, A., Ilyin, Y., Titov, K., 2013. Time domain spectral induced polarization of disseminated electronic conductors: laboratory data analysis through the Debye decomposition approach. J. Appl. Geophys. 98, 44–53.
Gurin, G., Titov, K., Ilyin, Y., Tarasov, A., 2015. Induced polarization of disseminated electronically conductive minerals: a semi-empirical model. Geophys. J. Int. 200 (3), 1555–1565.
Haario, H., Saksman, E., Tamminen, J., 1999. Adaptive proposal distribution for random walk Metropolis algorithm.
Haario, H., Saksman, E., Tamminen, J., 2001. An adaptive Metropolis algorithm. Bernoulli 7 (2), 223–242.
Hastings, W.K., 1970. Monte Carlo sampling methods using Markov chains and their applications. Biometrika 57 (1), 97–109.
Helt, K.M., Williams-Jones, A.E., Clark, J.R., Wing, B.A., Wares, R.P., 2014. Constraints on the Genesis of the Archean Oxidized, Intrusion-Related Canadian Malartic Gold Deposit, Quebec, Canada. Econ. Geol. 109 (3), 713–735.
Johnson, I.M., 1984. Spectral induced polarization parameters as determined through time-domain measurements. Geophysics 49 (11), 1993–2003.
Keery, J., Binley, A., Elshenawy, A., Clifford, J., 2012. Markov-chain Monte Carlo estimation of distributed Debye relaxations in spectral induced polarization. Geophysics 77 (2), E159–E170.

Kruschwitz, S., Binley, A., Lesmes, D., Elshenawy, A., 2010. Textural controls on low-frequency electrical spectra of porous media. Geophysics 75 (4), WA113–WA123.
Leroy, P., Revil, A., Kemna, A., Cosenza, P., Ghorbani, A., 2008. Complex conductivity of water-saturated packs of glass beads. J. Colloid Interface Sci. 321 (1), 103–117.
Lesmes, D.P., Morgan, F.D., 2001. Dielectric spectroscopy of sedimentary rocks. J. Geophys. Res.: Solid Earth 106 (B7), 13329–13346.
Macnae, J., 2015. Comment on: Tarasov, A. & Titov, K., 2013, On the use of the ColeCole equations in spectral induced polarization, Geophys. J. International, 195, 352356. Geophysical Journal International Jul. 202 (1). pp. 529–532.
Metropolis, N., Rosenbluth, A.W., Rosenbluth, M.N., Teller, A.H., Teller, E., 1953. Equation of state calculations by fast computing machines. J. Chem. Phys. 21, 1087–1092.
Misra, S., Torres-Verdín, C., Revil, A., Rasmus, J., Homan, D., 2016a. Interfacial polarization of disseminated conductive minerals in absence of redox-active species Part 1: mechanistic model and validation. Geophysics 81 (2), E139–E157.
Misra, S., Torres-Verdín, C., Revil, A., Rasmus, J., Homan, D., 2016b. Interfacial polarization of disseminated conductive minerals in absence of redox-active species. Part 2: effective electrical conductivity and dielectric permittivity. Geophysics 81 (2), E159–E176.
Morgan, F.D., Lesmes, D.P., 1994. Inversion for dielectric relaxation spectra. J. Chem. Phys. 100 (1), 671–681.
Niu, Q., Revil, A., 2016. Connecting complex conductivity spectra to mercury porosimetry of sedimentary rocks. Geophysics 81 (1), E17–E32.
Nordsiek, S., Weller, A., 2008. A new approach to fitting induced-polarization spectra. Geophysics 73 (6), F235–F245.
Patil, A., Huard, D., Fonnesbeck, C.J., 2010. PyMC: bayesian stochastic modelling in python. J. Stat. Softw. 35 (4), 1–81.
Pelton, W.H., Ward, S.H., Hallof, P.G., Sill, W.R., Nelson, P.H., 1978. Mineral discrimination and removal of inductive coupling with multifrequency IP. Geophysics 43 (3), 588–609.
Perrouty, S., Gaillard, N., Piette-Lauzière, N., Mir, R., Bardoux, M., Olivo, G.R., Linnen, R.L., Bérubé, C.L., Lypaczewski, P., Guilmette, C., Feltrin, L., Morris, W.A., 2017. Structural setting for Canadian Malartic style of gold mineralization in the Pontiac Subprovince, south of the Cadillac Larder Lake Deformation Zone, Québec, Canada. Ore Geol. Rev. 84, 185–201.
Placencia-Gomez, E., Slater, L., Ntarlagiannis, D., Binley, A., 2013. Laboratory SIP signatures associated with oxidation of disseminated metal sulfides. J. Contam. Hydrol. 148, 25–38.
Placencia-Gomez, E., Parviainen, A., Slater, L., Leveinen, J., 2015. Spectral induced polarization (SIP) response of mine tailings. J. Contam. Hydrol. 173, 8–24.
Raftery, A.E., Lewis, S., 1992. How Many Iterations in the Gibbs Sampler? In: Bayesian Statistics 4. Oxford University Press, pp. 763–773.
Revil, A., Florsch, N., 2010. Determination of permeability from spectral induced polarization in granular media. Geophys. J. Int. 181 (3), 1480–1498.
Revil, A., Koch, K., Holliger, K., 2012. Is it the grain size or the characteristic pore size that controls the induced polarization relaxation time of clean sands and sandstones? Water Resour. Res. 48 (5), W05602.
Revil, A., Florsch, N., Camerlynck, C., 2014. Spectral induced polarization porosimetry. Geophys. J. Int. 198 (2), 1016–1033.
Revil, A., Florsch, N., Mao, D., 2015. Induced polarization response of porous media with metallic particles. Part 1: a theory for disseminated semiconductors. Geophysics 80 (5), D525–D538.
Roberts, G.O., Rosenthal, J.S., 2001. Optimal scaling for various Metropolis-Hastings algorithms. Stat. Sci. 16 (4), 351–367.
Roberts, G.O., Rosenthal, J.S., 2007. Coupling and ergodicity of adaptive Markov chain Monte Carlo algorithms. J. Appl. Probab. 44 (2), 458–475.
Roberts, G.O., Gelman, A., Gilks, W.R., 1997. Weak convergence and optimal scaling of random walk Metropolis algorithms. Ann. Appl. Probab. 7 (1), 110–120.
Slater, L., Ntarlagiannis, D., Wishart, D., 2006. On the relationship between induced polarization and surface area in metal-sand and clay-sand mixtures. Geophysics 71 (2), A1–A5.
Tarantola, A., Valette, B., 1982. Generalized nonlinear inverse problems solved using the least squares criterion. Rev. Geophys. 20 (2), 219–232.
Tarasov, A., Titov, K., 2013. On the use of the Cole-Cole equations in spectral induced polarization. Geophys. J. Int. 195 (1), 352–356.
Vanhala, H., Peltoniemi, M., 1992. Spectral IP studies of Finnish ore prospects. Geophysics 57 (12), 1545–1555.
Vanhala, H., 1997. Mapping oil-contaminated sand and till with the Spectral Induced Polarization (SIP) Method. Geophys. Prospect. 45 (2), 303–326.
Vinegar, H.J., Waxman, M.H., 1984. Induced polarization of shaly sands. Geophysics 49 (8), 1267–1287.
Weigand, M., Kemna, A., 2016. Debye decomposition of time-lapse spectral induced polarisation data. Comput. Geosci. 86, 34–45.
Weller, A., Nordsiek, S., Debschütz, W., 2010a. Estimating permeability of sandstone samples by nuclear magnetic resonance and spectral-induced polarization. Geophysics 75 (6), E215–E226.
Weller, A., Slater, L., Nordsiek, S., Ntarlagiannis, D., 2010b. On the estimation of specific surface per unit pore volume from induced polarization: a robust empirical relation fits multiple data sets. Geophysics 75 (4), WA105–WA112.
Wong, J., 1979. An electrochemical model of the induced-polarization phenomenon in disseminated sulfide ores. Geophysics 44 (7), 1245–1265.
Zisser, N., Kemna, A., Nover, G., 2010. Relationship between low-frequency electrical properties and hydraulic permeability of low-permeability sandstones. Geophysics 75 (3), E131–E141.